

LDA+Slave-Boson approach to the correlated electronic structure of the metamagnetic bilayer ruthenate $\text{Sr}_3\text{Ru}_2\text{O}_7$

Christoph Piefke and Frank Lechermann*

I. Institut für Theoretische Physik, Universität Hamburg, D-20355 Hamburg, Germany

Received XXXX, revised XXXX, accepted XXXX

Published online XXXX

Key words: Strong correlation, electronic structure, metamagnetism, density functional theory

* Corresponding author: e-mail Frank.Lechermann@physnet.uni-hamburg.de, Phone: +49-40-428387943, Fax: +49-40-428386798

The combination of the local-density approximation (LDA) with the rotationally invariant slave-boson theory (RISB) is used to investigate the realistic correlated electronic structure of $\text{Sr}_3\text{Ru}_2\text{O}_7$. From Wannier-downfolding the low-energy band structure to a three-band model for the $\text{Ru}(t_{2g})$ states, the interacting problem is solved including intra- and inter-orbital Hubbard terms as well as spin-flip and pair-hopping interactions. Therewith it is possible to obtain valuable insight into the orbital occupations, relevant local spin multiplets and the fermiology with increasing correlation strength.

Besides generic correlation-induced band-narrowing and -shifting, an intriguing quasiparticle structure close to the Fermi level is found in the neighborhood of the notorious γ_2 pocket in the Brillouin zone. Along the $\Gamma-X$ direction in \mathbf{k} -space, that structure appears very sensitive to electronic self-energy effects. The subtle sensitivity, connected also its manifest multi-orbital character, may put this very low-energy structure in context with the puzzling metamagnetic properties of the compound.

Copyright line will be provided by the publisher

1 Introduction Strongly correlated electron systems are not only a fascinating research field from the viewpoint of fundamental research, but also become more and more of technological relevance in the context of the demand for specific high-responsive behavior. The very subtle balance between the kinetic-energy term and the Coulomb repulsion among the electrons in these systems indeed often result in e.g. absorbing magnetic, superconducting or thermoelectric properties. Concerning the theoretical description on an atomistic level, the standard Kohn-Sham (KS) band-theory representation of density functional theory (DFT) for the solid state is usually inappropriate for realistic materials with strong electronic correlations. For instance, the Mott-insulating state as an electron localization in real space amounts to a complete breakdown of the conventional band-structure concept, e.g., given by the local-density approximation (LDA) to DFT. However the simple LDA+U extension for the strongly correlated regime

is generally not well-suited for metals, since the correlated low-energy behavior close to the Fermi level ε_F cannot be captured within this static mean-field method.

Here we want to show that the combination of LDA with the slave-boson theory [1,2] in its rotationally-invariant form [3,4] (RISB) at saddle-point may be an efficient approach to model strongly correlated metals. This LDA+RISB scheme can account for many details of the quasiparticle (QP) physics close to ε_F of strongly interacting multi-orbital systems with modest effort compared to, e.g., numerically expensive Quantum-Monte-Carlo impurity computations within the framework of dynamical mean-field theory (DMFT).

In this work the electronic correlations effects in the complex $\text{Sr}_3\text{Ru}_2\text{O}_7$ compound shall be discussed within the LDA+RISB method. The puzzling ruthenate has gathered much attention in recent years due to its metamagnetic behavior at low temperatures, which may be related to a

Copyright line will be provided by the publisher

quantum critical point [5,6,7]. The paramagnetic Fermi-liquid displays one of the highest electronic specific heat values among oxides and has definitely to be placed in the strongly correlated regime. Because of its very delicate low-energy physics, the slave-boson technique, focussing on the strongly renormalized QP part, is an adequate framework for investigations beyond standard LDA approaches.

2 The Sr₃Ru₂O₇ compound The $n=2$ case of the multilayer Ruddlesden-Popper strontium ruthenates Sr _{$n+1$} Ru _{n} O _{$2n+3$} serves as an interesting application of our theoretical methodology. The perovskite end member SrRuO₃ ($n=\infty$) of this family is at low temperature T a ferromagnetic metal, whereas the also itinerant single-layered Sr₂RuO₄ compound is paramagnetic at ambient T and becomes superconducting below $T_c \sim 4.2$ K, with a widely believed triplet pairing [8]. The crystal structure of Sr₃Ru₂O₇ [9] with lattice parameters $a=b=5.5006\text{\AA}$ and $c=20.725\text{\AA}$ is based on the orthorhombic space group $Bbcb$ (#68) (see Fig. 1) and does not show the fourfold symmetry of the simpler Sr₂RuO₄ structure. It consists of RuO₂ bilayers, whereby the RuO₆ octahedra are rotated by 6.8° . The unit cell exhibits four Ru ions, all equivalent by symmetry.

Many experiments show that the Sr₃Ru₂O₇ compound is located just at the paramagnetic-to-ferromagnetic transition boundary. It is still paramagnetic in zero magnetic field, but positioned very close to the ferromagnetic instability [10]. The system shows strongly renormalized Fermi-liquid behavior with however a strong resistivity anisotropy $\rho_c/\rho_{ab} \sim 100$ [10]. With applied magnetic field H , the systems shows metamagnetic behavior, i.e., a very large $\partial M/\partial H$, around $H=5.5(7.7)\text{T}$ for $H||ab(c)$ [11]. Furthermore this metamagnetic region may be associated with being in the neighborhood of a quantum critical point that can be approached via tuning the magnetic-field angle with the ab plane [12]. Reachable within fields $H < 10$ T, the physics of this metamagnetism is acting on a very low energy scale of the order of a few meV. Note also that the Fermi-liquid regime in vanishing field exists below 10-15 K, however can be driven to zero temperature with applied field [5].

3 Theoretical Approach In the present modeling we combine the LDA approach to DFT with the rotationally invariant slave-boson theory at saddle-point. For the LDA part, we utilized an implementation [13] of the highly-accurate mixed-basis pseudopotential (MBPP) technique [14]. This band-structure code employs norm-conserving pseudopotentials [15] and an efficient mixed basis consisting of plane waves and a few localized orbitals. Scalar-relativistic pseudopotentials and the LDA exchange-correlation functional after Perdew and Wang [16] were used in the actual computations.

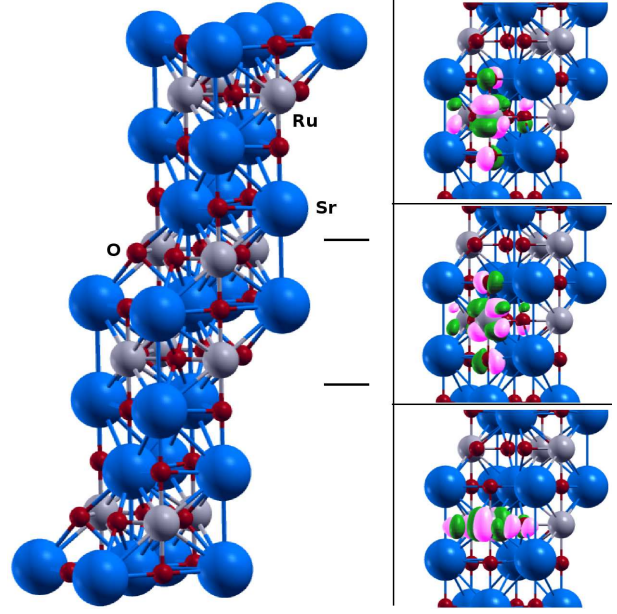


Figure 1 Left: crystal structure of the orthorhombic $Bbcb$ -Sr₃Ru₂O₇, where the Ru bilayer part is indicated within the dark lines. Right from top to bottom: d_{yz} , d_{xz} and d_{xy} effective Wannier function derived from the LDA band structure.

Based on the LDA electronic structure a low-energy KS dispersion $\varepsilon_{\mathbf{k}}^{(KS)}$ for each wave vector \mathbf{k} within the t_{2g} manifold of Sr₃Ru₂O₇ is constructed via maximally-localized Wannier functions (MLWF) [17, 18] for the four Ru ions in the orthorhombic unit cell. This effective single-particle 12×12 Hamiltonian is then supplemented by on-site Coulomb interactions, resulting in additional Hubbard, exchange, spin-flip and pair-hopping terms on each Ru ion i with t_{2g} -orbital indices m, m' in the unit cell α . The interacting problem hence reads:

$$H = \sum_{\mathbf{k}mm'\sigma} \varepsilon_{\mathbf{k}mm'}^{(KS)} d_{\mathbf{k}m\sigma}^\dagger d_{\mathbf{k}m'\sigma} + \sum_{\alpha} H_{\alpha}^{(loc)} \quad , \quad (1)$$

with the local interacting part in the unit cell given by three-orbital generalized Hubbard model on each Ru site, i.e.,

$$H_{\alpha}^{(loc)} = U \sum_{im} n_{im\uparrow} n_{im\downarrow} + \frac{1}{2} \sum_{i,m \neq m',\sigma} \left\{ U' n_{im\sigma} n_{im'\bar{\sigma}} + U'' n_{im\sigma} n_{im'\sigma} + J d_{im\sigma}^\dagger d_{im'\bar{\sigma}}^\dagger d_{im\bar{\sigma}} d_{im'\sigma} + J_C d_{im\sigma}^\dagger d_{im\bar{\sigma}}^\dagger d_{im'\bar{\sigma}} d_{im'\sigma} \right\} \quad (2)$$

with $n=d^\dagger d$. The first term in eq. (2) marks the intra-orbital Coulomb interaction with Hubbard U , the second term the inter-orbital Hund's rule corrected interaction with $U'=U-J$ and $U''=U-2J$ for unequal and equal spin ori-

entiation $\sigma=\uparrow, \downarrow$, respectively. Finally, the third term accounts for spin-flip and the fourth term for pair-hopping processes, where we used $J_C=J$ for the real MLWFs.

For the solution of the problem posed by eq. (1) the RISB method was employed, where the electron operator $d_{i\mu\sigma}\equiv d_{\mu\sigma}$ is represented as $\underline{d}_{\mu\sigma}=\hat{R}[\phi]_{\mu\mu'}^{\sigma\sigma'}f_{\mu'\sigma'}$. Here \hat{R} is a non-diagonal transformation operator that relates the physical operator to the QP operator $f_{\mu\sigma}$ and is written in terms of the slave bosons $\{\phi_{An}\}$. In this generalized slave-boson theory ϕ carries the index A for the physical-electron state and n for the QP Fock state. In the end, the general idea is to rewrite eq. (2) solely in terms of slave-boson operators which allows to integrate out the QP part. The operator decomposition into QP and interacting slave-boson part introduces two constraints, namely

$$\sum_{An} \phi_{An}^\dagger \phi_{An} = 1 \quad , \quad (3)$$

$$\sum_{Ann'} \phi_{An'}^\dagger \phi_{An} \langle n | f_{\mu\sigma}^\dagger f_{\mu'\sigma'} | n' \rangle = f_{\mu\sigma}^\dagger f_{\mu'\sigma'} \quad , \quad (4)$$

whereby eq. (3) normalizes the total boson weight to unity and eq. (4) ensures that QP and boson contents match at every site i . This selection of the physical states is imposed through a set of Lagrange multipliers $\{\lambda\}$. In the mean-field version at saddle-point these constraints hold on average, with the bosons condensed to c numbers. The numerical effort amounts to the solution of the saddle-point equations for $\{\phi\}$, $\{\lambda\}$ (see Ref. [4] for further details). In the calculations we also used the set of local Fock states $\{|n\rangle\}$ for the set of atomic states $\{A\}$ on each Ru ion. It is important to note in this context that in the present work no inter-site slave bosons were introduced. Thus at the saddle-point, the RISB physical self-energy of the d electrons is given by [4]

$$\Sigma_d^i(\omega) = \omega (1 - \mathbf{Z}^{-1}) + [\mathbf{R}^\dagger]^{-1} \mathbf{\Lambda} \mathbf{R}^{-1} - \varepsilon^{(0)} \quad , \quad (5)$$

diagonal in the Ru sites. Here $\mathbf{Z}=\mathbf{R}\mathbf{R}^\dagger$ is the QP-weight matrix and $\mathbf{\Lambda}$ is the lagrange-multiplier matrix. The quantity $\varepsilon^{(0)}$ denotes a possible one-body term in the k -summed KS-Hamiltonian, which should not appear in the QP part of the framework. Thus Σ_d contains a term linear in frequency and a static part. Though more approximative than more involved methods like, e.g., quantum Monte-Carlo, which may handle the full frequency dependence, this proves sufficient in many cases to describe the QP physics at low-energy. It also provides additional insight into local excitations within a static self-energy approximation. In this regard, the slave-boson amplitudes yield direct access to the occupation of local multiplets in the metallic state. The RISB mean-field approach may therefore be seen as meaningful simplified approximation to correlated metals beyond LDA. Note that it is superior to LDA+U in this regime, since the latter is designed for Mott-insulating systems.

Our application of LDA+RISB to $\text{Sr}_3\text{Ru}_2\text{O}_7$ considers no spin-orbit-coupling (SOC) effects. Albeit SOC is be-

lieved to be important for the low-energy physics of this compound, the present study shall exhibit that many interesting features of the correlated electronic structure may already be revealed without that coupling. Further studies including the SOC with the obviously well-tailored RISB method will be discussed in a future work.

4 Results and discussion

4.1 LDA electronic structure The Ru ions in the $\text{Sr}_3\text{Ru}_2\text{O}_7$ compound are formally in the $4+$ state, i.e. the $4d$ shell of the transition metal is filled with four electrons. Since the system is known to be in the low-spin state, all these electrons are located in the t_{2g} manifold. Many issues of the electronic structure on the LDA level have already been discussed in previous studies [19, 20, 21], albeit the very low-energy regime has not been addressed theoretically in great detail.

Figure 2 shows the LDA band structure close to the Fermi level, consisting mainly of an Ru(t_{2g}) dominated 12-band manifold. The dispersion is strongly two-dimensional, although still some bands display significant variation along $\Gamma-A$ in the first Brillouin zone (BZ). There are several rather flat bands close to ε_F , especially in the neighborhood of the X point, as also observed in recent angle-resolved photoemission (ARPES) experiments [21, 22]. Additionally shown in Fig. 2 are the effective bands from the MLWF construction, which are in very good agreement with the original LDA bands close to zero energy. Due to the strong hybridization of the d_{xy} orbital with oxygen states at energies below -2 eV, the effective Wan-

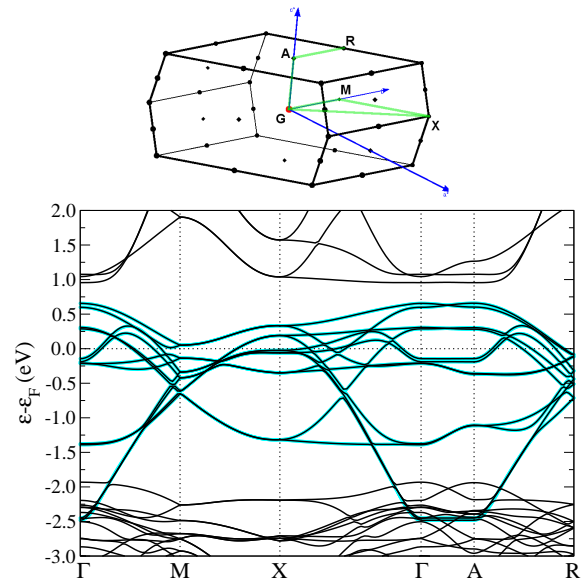


Figure 2 Brillouin zone with selected high-symmetry points (top). The green line marks the chosen path for the LDA band structure (bottom) including the downfolded effective Wannier t_{2g} low-energy bands (cyan/grey lines).

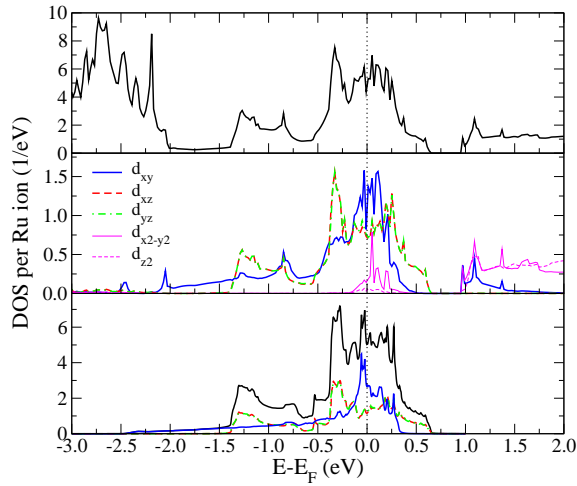


Figure 3 LDA density of states normalized to one Ru ion. Top: total DOS, middle: local Ru- d DOS within $r_{\text{Ru}}=2.0$ a.u.. Bottom: effective Wannier t_{2g} low-energy DOS. Note that the t_{2g} Wannier functions are tailored to match the LDA bands and are thus to some extent build on linear combinations of the original d states shown in the middle part.

nier manifold ranges from -2.5 eV to 0.6 eV, i.e., displays a bandwidth of about 3.1 eV.

More details of the LDA spectral behavior of the Ru($4d$) states may be extracted from the density-of-states (DOS) plot in Fig. 3. It is first observable that the Fermi level resides actually between prominent peaks within the total DOS of the system. Projecting the local DOS onto the standard cubic d harmonics along the cartesian axes renders the dominant behavior of the t_{2g} manifold at low energy obvious. Thereby the in-plane d_{xy} orbital has more substantial structure close to E_F than the nearly degenerate d_{xz}, d_{yz} orbitals. Interestingly, the e_g orbital $d_{x^2-y^2}$ has also some appreciable weight in that energy regime, with important overall clear signatures of hybridization with the d_{xy} orbital. The effective Wannier DOS reproduces well the low-energy regime, but note that the obtained t_{2g} -only Wannier orbitals are now not aligned along the cartesian axes anymore, but show some tilting in line with the orthorhombic distortions of the Bbc structure. Furthermore especially the effective d_{xy} -like orbital is now “dressed” with the $d_{x^2-y^2}$ hybridization just mentioned. This is indeed visible in the contour plot of the former Wannier orbital exhibited in Fig. 4, which also shows the slight tilting in the xy plane parallel to the RuO_2 bilayer. Note that from the underlying MLWF construction the on-site energy of the d_{xy} -like orbital is higher than for the d_{xz}, d_{yz} -like by about 115 meV.

4.2 LDA+RISB modeling In order to account for electronic on-site correlations beyond LDA we introduced the local Hamiltonian (2) on each Ru site and solved the

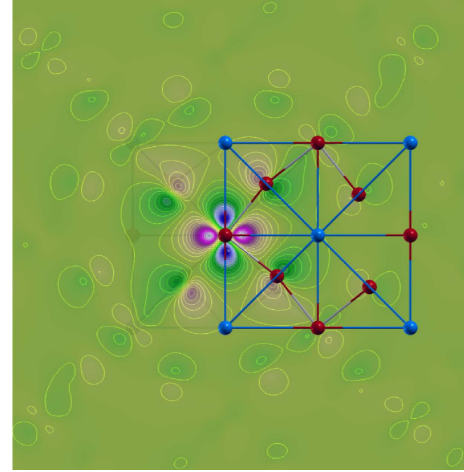


Figure 4 Isolines of the d_{xy} -like Wannier function. The x - and y -axis correspond to the diagonals of the plot. The Ru ion associated to the plotted MLWF resides below the (red) oxygen ion.

interacting problem (1) with the KS t_{2g} -like Wannier dispersions discussed in the last section. In the following we will refer to the latter by $d_{xz,yz,xy}$, albeit it is understood that the effective orbitals are tailored to Bbc - $\text{Sr}_3\text{Ru}_2\text{O}_7$ through the present MLWF construction. The $d_{xz,yz}$ are only nearly degenerate, but in the discussion the orbitally averaged data is shown, since the present orbital-resolved results differ only marginally. Note however that the calculations allowed for the full differences between all the treated local orbitals. According to theoretical estimates for the ruthenates [23, 24, 25], the value of the Hund’s coupling was set to $J=0.35$ eV for all the computations. While there are LDA+DMFT investigations for Sr_2RuO_4 with values for the Hubbard U between 1-3 eV [23, 26, 25], to

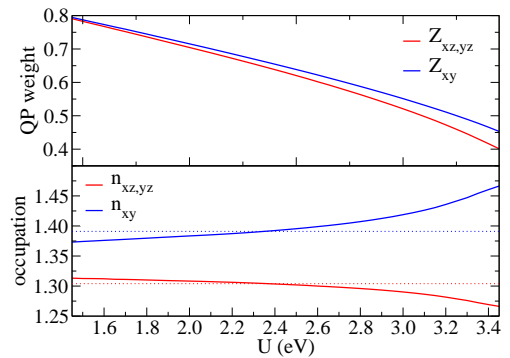


Figure 5 Top: Orbital-dependent QP weight (top) and orbital occupations per Ru ion (bottom) with increasing U for the t_{2g} states. The dotted line in the bottom part marks the respective occupation for $U=0$.

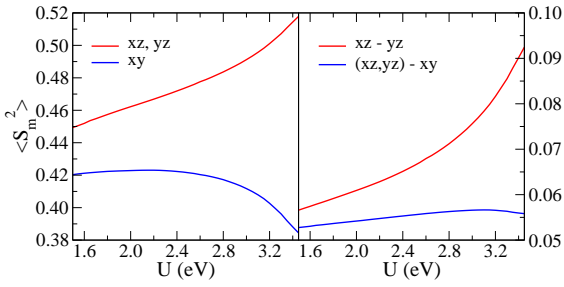


Figure 6 Local intra- and inter-orbital spin correlations with increasing U .

our knowledge no such approach exists to $\text{Sr}_3\text{Ru}_2\text{O}_7$. Yet optics experiments [27] point towards a similar U value. Here we scanned the onsite Coulomb interaction up to $U=3.45$ eV, since it is also known that due to the neglect of quantum fluctuations in slave-boson approaches, the effect of U may be underestimated [28].

Figure 5 shows the diagonal QP weight Z_{mm} for $m=(xz, yz), xy$ with respect to U . The inter-orbital terms $Z_{mm'}$ remain marginal and appear irrelevant in the present orbital representation. It is seen that moderate U values already provide a significant QP renormalization. The latter is smaller for the d_{xy} orbital, understandable from the larger orbital-resolved bandwidth. In addition, Fig. 5 displays the orbital- and U -dependent occupations for the total four electrons on each Ru ion. As explainable from the lower crystal-field level, the d_{xy} orbital is stronger occupied in the noninteracting case. It may be observed that the affect of U on the occupations is rather subtle, with compensating/polarizing tendencies below/above $U^* \sim 2.35$ eV. Note of course that the latter value depends strongly on the chosen value for J . Though the correlation-induced interorbital charge transfers are not dramatic, one may still expect impact on the very sensitive low-energy physics of $\text{Sr}_3\text{Ru}_2\text{O}_7$.

According to Hund's rule, in an atomic picture the Ru ion should have $S=1$ with the d_{xy} orbital being doubly occupied on the basis of the given crystal-field splitting. Our calculations indeed show that $S^2=S(S+1)$ increases from $S^2 \sim 1$ at $U=0$ towards $S^2 \sim 1.83$ for $U=3.45$ eV. In this respect, the orbital-resolved local spin correlations are shown in Fig. 6, with the anticipated different behavior for d_{xy} and $d_{xz,yz}$. Namely, $S_{xz,yz}^2$ grows strongly with U , whereas S_{xy}^2 diminishes substantially after U^* in order to cope with the formation of the local spin pair in that orbital. Also the inter-orbital spin correlations show the designated xz - yz spin-parallel coupling. Another option to investigate the local spin states is given by an inspection of the slave-boson weights $|\phi_{\Gamma\Gamma'}|^2$ within the local $\text{Ru}(t_{2g})$ multiplet basis $\{\Gamma\}$. Therefore the slave-boson amplitudes $\phi_{nn'}$ are rotated in the eigenbasis of the isolated local Hamiltonian (2) via

$$\phi_{\Gamma\Gamma'} = \mathcal{U}_{\Gamma n}^\dagger \phi_{nn'} \mathcal{U}_{n'\Gamma'} \quad , \quad (6)$$

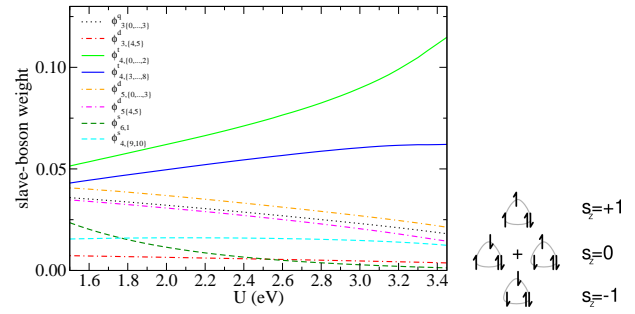


Figure 7 Left: Weights of the local multiplets on a given Ru ion via the symmetry-adapted slave-boson amplitudes squared $|\phi_{\Gamma\Gamma'}|^2$ with U . Right: Fock decomposition of the dominant threefold degenerate triplet state $\Gamma_{4,\{0,\dots,2\}}^t$, where d_{xy} is the doubly-occupied orbital.

where $\mathcal{U}_{n\Gamma}$ provides the unitary mapping between the multiplet basis $\{\Gamma\}$ and the Fock basis $\{n\}$. We denote a specific multiplet by $\Gamma_{p,r}^m$, where p describes the particle sector, r the energy level therein (starting with $n=0$ for the respective ground state) and m marks the spin state, i.e., singlet 's', doublet 'd', triplet 't' and quartet 'q'. The diagonal multiplet weights $|\phi_{\Gamma\Gamma'}|^2$ are plotted in Fig. 7 with respect to U . Note that in the present case the $\phi_{\Gamma\Gamma'}$ are close to diagonal with only few off-diagonal terms of minor amplitude. It is seen that the local physics is dominated by a threefold-degenerate triplet state in the four-particle sector with d_{xy} indeed being the doubly-occupied orbital. Beyond that one, two other triplets with only marginal energy difference follow and then already a five-particle doublet shows up relevant, however losing weight with increasing U .

Besides affecting the local states, the electronic correlations introduced by U and J of course also have impact on the QP dispersions. From eq. (5) it follows that the RISB self-energy narrows the bands via Z and gives rise to band shifts through the remaining static term. In Fig. 8 we compare the Fermi surface (FS) in LDA ($U=0$) with the case for $U=3.45$ eV. In general the FS is rather complex with in total six sheets, labeled $\delta, \alpha_1, \alpha_2, \gamma_1, \beta$ and γ_2 (see e.g. Ref. [21]). The LDA FS is in rather good agreement with ARPES data [21]. The overall appearance bears the prominent quasi-two-dimensional character of the compound with only weak FS warping along c^* , especially for the sheets in the inner area of the BZ. However there are also bands crossing the Fermi level along c^* close to the zone boundary, e.g. from $M-R$. This observation may be important for an understanding of the apparent metallic behavior of the measured optical conductivity along c [29]. The interacting FS shows for the chosen U value no dramatic differences, which is expected since it is well known that LDA provides a surprisingly good fermiology for many strongly correlated metals. However there are still some important changes that may shed some further

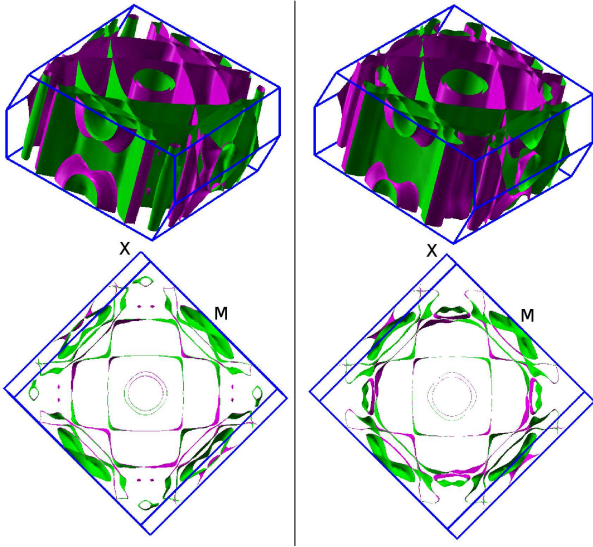


Figure 8 Fermi surface of $\text{Sr}_3\text{Ru}_2\text{O}_7$ for $U=0$ (left) and $U=3.45$ eV (right). In the bottom the view along the c^* axis in k -space is depicted.

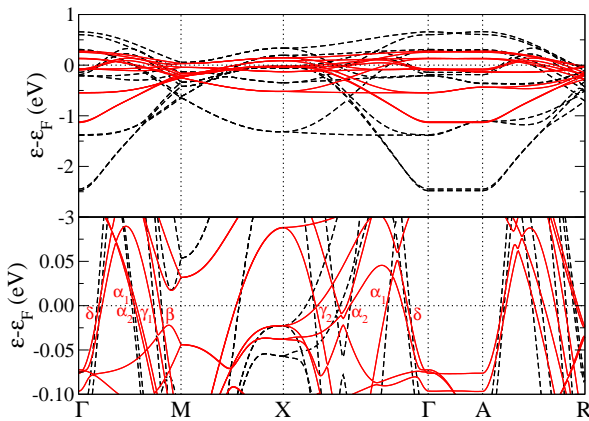


Figure 9 LDA (dashed lines) and renormalized QP bands ($U=3.45$ eV) along the high-symmetry directions. The lower part shows a blow up around the Fermi level ε_F with the FS sheets δ , α_1 , α_2 , γ_1 , β and γ_2 .

light on the generic low-energy physics of $\text{Sr}_3\text{Ru}_2\text{O}_7$. The renormalized FS can partly also be studied from the deviations of the associated bands crossing ε_F along the high-symmetry lines in the BZ, as displayed in Fig. 9. For most of the sheets there are some minor size changes with U (which should be in overall accordance with Luttinger’s theorem), e.g., δ , α_1 and α_2 somewhat growing in the $k_z=0$ plane. However the γ_2 pocket is rather severely modified. First of all from ARPES experiment, γ_2 appears as a small but “simple” hole pocket more or less right inbetween the α_2 sheet boundary and the X point along the $\Gamma-X$ direction [21]. On the other hand, the computed (QP) band

structure in this region looks rather complex, with possibly as many as four Fermi-level crossings. Intriguingly, those crossings pair into two with two bands crossing each other in an “dirac-cone-manner”, respectively (cf. Fig. 9). As it turns out, this low-energy structure is very sensitive to electronic correlations and depending on the interaction strength, the two named crossing twofolds shift between hole- or electron-like fermiology. In the LDA case the twofold close to X is higher in energy, giving rise to a hole pocket as observed in experiment, whereas the twofold close to α_2 is barely shifted into the electron-pocket appearance. For $U=3.45$ eV the situation is nearly reversed for the former pocket part, while the latter becomes stabilized in what’s now a sizeable electron pocket. Note that since being close to the γ_2 -pocket structure also the α_2 sheet in the $\Gamma-X$ direction is affected by the low-energy correlation-induced restructuring. This results in a stronger renormalization of the α_2 sheet in that direction compared to the one along $\Gamma-M$, which is in agreement with findings in recent ARPES experiments [22].

Surely, this whole discussion depends on the magnitude of U and J , however already the fact that underneath the γ_2 pocket hides such a correlation-sensitive low-energy structure may be of greater importance. The reason for the sensitivity is besides the flatness of the associated bands close to the X point given by the fact that while the two hole-like bands of the outlined fourfold are dominantly d_{xy} , the electron-like bands are mainly $d_{xz,yz}$. Thus the multi-orbital character of the compound directly manifests in the complex structure around the γ_2 pocket. In the experimental dispersions [21] the described low-energy γ_2 structure is partly visible in the occupied area, however much more strongly renormalized (lowest-energy band ~ 1 meV). The effect of SOC, especially via additional band splittings, may here be important to reveal more details of this low-energy segment. In addition, the renormalization effect through quantum spin fluctuations could be relevant

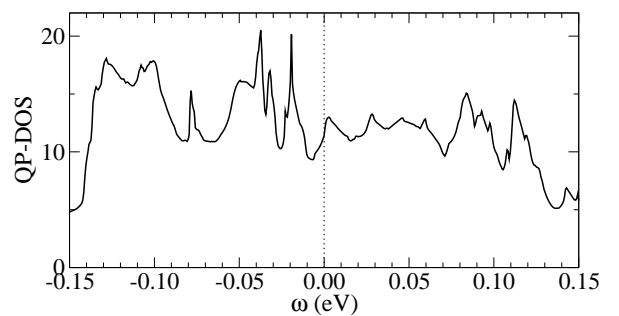


Figure 10 RISB QP density of states for the t_{2g} states per Ru ion ($U=3.45$ eV). Note that the absolute value is somewhat artificial due to the not-described Hubbard bands in the spectral function within slave-boson mean-field and should not be directly related to experimental values.

in the system since its prone to the ferromagnetic instability.

Finally, we show in Fig. 10 the QP DOS from the LDA+RISB calculation in a small energy window around ε_F . Albeit we obviously can not fully reach in the present modeling the very low-energy scale seen in experiment, it is observable that already here a rather subtle energy structure shows up in a small range around ε_F . The latter value resides for $U=3.45$ eV within a slope of width ~ 10 meV and onset 6 meV below zero energy. Note that a large number of unoccupied states above ε_F is also verified from ARPES measurements [21].

5 Conclusions The present work dealt with a realistic LDA+RISB approach to the low-energy electronic structure of the puzzling $\text{Sr}_3\text{Ru}_2\text{O}_7$ compound. It was shown that the LDA band structure close to the Fermi level can be accurately downfolded to an effective MLWF description with tailored t_{2g} -like orbitals. Supplemented by generic on-site Coulomb correlations, the resulting interacting model accounts for strong electronic self-energy effects. A dominant filling of the d_{xy} orbital was identified, locally favoring a corresponding four-particle triplet state at larger Hubbard U . The renormalization of the low-energy electronic structure singles out the γ_2 pocket (and its neighborhood) as especially sensitive to electronic correlations, also due to its manifest multi-orbital character. In view of the very low energy scale close to the X point this observation draws much attention to that pocket as a possible key object for the understanding of metamagnetism in $\text{Sr}_3\text{Ru}_2\text{O}_7$ [30]. Albeit the Hubbard parameters have been chosen more or less by hand in this study, the mere fact that one may here find definite regions in \mathbf{k} -space that are rather prominently susceptible to electronic correlations seems an interesting result that deserves further detailed investigation. The neglect of SOC is a sure drawback of the present study, but because of the already good data agreement between experiment and theory on, e.g., the Fermi surface, very strong changes of the current results are not expected with including SOC effects. The latter will be of course important when turning on a magnetic field H , especially when elaborating on the influence of the angle-dependence thereof. However the RISB formalism is in principle ideally suited to cope with such physics and we plan to address it in a future work. For instance, the orbital-occupation shifts in the correlated regime with respect to an angle-dependent field, possibly close to the metamagnetic response, would be of vital interest.

Acknowledgements Financial support from the Free and Hanseatic City of Hamburg in the context of the NANOSPIN-TRONICS Landesexzellenzinitiative is gratefully acknowledged. Computations were performed at the North-German Supercomputing Alliance (HLRN).

References

- [1] P. Coleman, Phys. Rev. B **29**, 3035 (1984).
- [2] G. Kotliar and A. E. Ruckenstein, Phys. Rev. Lett. **57**, 1362 (1986).
- [3] T. Li, P. Wölfle, and P. J. Hirschfeld, Phys. Rev. B **40**, 6817 (1989).
- [4] F. Lechermann, A. Georges, G. Kotliar, and O. Parcollet, Phys. Rev. B **76**, 155102 (2007).
- [5] S. A. Grigera, R. S. Perry, A. J. Schofield, M. Chiao, S. R. Julian, G. G. Lonzarich, S. I. Ikeda, Y. Maeno, A. J. Millis, and A. P. Mackenzie, Science **294**, 329 (2001).
- [6] P. Gegenwart, F. Weickert, M. Garst, R. S. Perry, and Y. Maeno, Phys. Rev. Lett. **96**, 136402 (2006).
- [7] R. A. Borzi, S. A. Grigera, J. Farrell, R. S. Perry, S. J. S. Lister, S. L. Lee, D. A. Tennant, Y. Maeno, and A. P. Mackenzie, Science **315**, 214 (2006).
- [8] A. P. Mackenzie and Y. Maeno, Rev. Mod. Phys. **75**, 657 (2003).
- [9] H. Shaked, J. D. Jorgensen, O. Chmaissem, S. Ikeda, and Y. Maeno, J. Solid State Chem. **154**, 361 (2000).
- [10] S. I. Ikeda, Y. Maeno, S. Nakatsuji, M. Kosaka, and Y. Uwatoko, Phys. Rev. B **62**, R6089 (2000).
- [11] R. S. Perry, L. M. Galvin, S. A. Grigera, L. Capogna, A. J. Schofield, A. P. Mackenzie, M. Chiao, S. R. Julian, S. I. Ikeda, S. Nakatsuji, and Y. Maeno, Phys. Rev. Lett. **86**, 2661 (2001).
- [12] S. A. Grigera, R. A. Borzi, A. P. Mackenzie, S. R. Julian, R. S. Perry, and Y. M. and, Phys. Rev. B **67**, 214427 (2003).
- [13] B. Meyer, C. Elsässer, F. Lechermann, and M. Fähnle, FORTRAN 90 Program for Mixed-Basis-Pseudopotential Calculations for Crystals, Max-Planck-Institut für Metallforschung, Stuttgart, unpublished.
- [14] S. G. Louie, K. M. Ho, and M. L. Cohen, Phys. Rev. B **19**, 1774 (1979).
- [15] D. Vanderbilt, Phys. Rev. B **32**, 8412 (1985).
- [16] J. P. Perdew and Y. Wang, Phys. Rev. B **45**, 13244 (1992).
- [17] N. Marzari and D. Vanderbilt, Phys. Rev. B **56**, 12847 (1997).
- [18] I. Souza, N. Marzari, and D. Vanderbilt, Phys. Rev. B **65**, 035109 (2001).
- [19] I. Hase and Y. Nishihara, J. Phys. Soc. Jpn. **66**, 3517 (1997).
- [20] D. Singh and I. I. Mazin, Phys. Rev. B **63**, 165101 (2001).
- [21] A. Tamai, M. P. Allan, J. F. Mercure, W. Meevasana, R. Dunkel, D. H. Lu, R. S. Perry, A. P. Mackenzie, D. J. Singh, Z. X. Shen, and F. Baumberger, Phys. Rev. Lett. **101**, 026407 (2008).
- [22] J. Lee, M. P. Allan, M. A. Wang, J. Farrell, S. A. Grigera, F. Baumberger, J. C. Davis, and A. P. Mackenzie, Nat. Phys. **5**, 800 (2009).
- [23] A. Liebsch and A. Lichtenstein, Phys. Rev. Lett. **84**, 1591 (2000).
- [24] S. Okamoto and A. J. Millis, Phys. Rev. B **70**, 195120 (2004).
- [25] J. Mravlje, M. Aichhorn, T. Miyake, K. Haule, G. Kotliar, and A. Georges, arXiv:1010.5910v1 (2010).
- [26] Z. V. Pchelkina, I. A. Nekrasov, T. Pruschke, A. Sekiyama, S. Suga, V. I. Anisimov, and D. Vollhardt, Phys. Rev. B **75**, 035122 (2007).
- [27] A. V. Puchkov, M. C. Schabel, D. N. Basov, T. S. Abd G. Cao, T. Timusk, and Z. X. Shen, Phys. Rev. Lett. **81**, 2747 (1998).

- [28] D. Grieger, L. Boehnke, and F. Lechermann, *J. Phys.: Condens. Matter* **22**, 275601 (2010).
- [29] C. Mirri, L. Baldassarre, S. Lupi, M. Ortolani, R. Fittipaldi, A. Vecchione, and P. Calvani, *Phys. Rev. B* **78**, 155132 (2008).
- [30] C. M. Puetter, J. G. Rau, and H. Y. Kee, *Phys. Rev. B* **81**, 081105(R) (2010).